Investigation of Katabatic Winds on Belledonne

Jakob Siedersleben

Master 1 Applied Mechanics
Supervisor: Jean-Emmanuel Sicart

Université Grenoble Alpes
May 2018

Contents

Acknowledgement

I would like to thank Jean-Emmanuel Sicart for his patience, support and his supervision during this project and all the other professors who helped me. Obviously all the colleagues and friends who support me with helpful advice and company throughout this year and last but never least my parents without them none of this would be possible.

Abstract

The first investigations on katabatic winds already took place in the 1840's. Poulos and Thong, 2008 described them the following way: "These winds, which flow down the topographic gradient as a result of surface cooling, provide a major transport and dispersion mechanism in mountainous regions and affect the energy exchange between the earth's surface and the atmosphere." Although these winds have been under investigation for so long there is still need for new data to improve the understanding and the accuracy of computational models. Especially the examination of these winds on steep slopes is due to hardly accesible terrain and heavy, expensive equipment a task which has not be done very often, which is why there exist hardly any scientific paper on this subject.
For this reason measurements on a steep (20°-40°) slope on the western side of the Grand Colon located a few kilometers east of Grenoble were executed in the year 2015 by Philibert Alban. The data of these measurements allow us to have a closer look on the structure and characteristics of these winds and to explain the surface fluxes of momentum, the sensible heat flux. In addition the influence of the steep slope on the production/destruction of turbulence was investigated.

1 Introduction

Winds appearing on sloped areas play an important role in meteorology, in climate and in the transport of pollutants in cities in mountainous regions. These thermal winds can be distinguished in two different types: Upslope (anabatic) winds, appearing due to the solar heating of the ground and downslope (katabatic) winds, appearing due to the cooling of the ground most of all at night and in hibernal conditions (Mahrt, 2014). In fact, the conditions were katabatic winds appear are the same which promote high air pollution in cities surrounded by mountain such as Grenoble or the valley of Chamonix, which are known for their high pollution levels compared to the rest of France. But the measurement and documentation of these winds is still a challenge not at last, because there does not exist a lot of detailed usable data and executing measurments in mountanious areas is due to heavy equipment and terrain which is difficult to approach very difficult. (Philibert, 2016)
The goal of this research project is to improve the understanding of these thermal downward winds on steep (20°-40°) mountain slopes. For this reason measurements on the east side of the Grand Colon taking part from 07/04/1015 to 22/04/2015 were investigated. The observations included low frequency measurements and high frequency measurements which allow us to have a look on the structure and characteristics of these winds and to explain the driving forces of this jet with the help of the flux of momentum, the sensible heat flux, the turbulence kinetic energy (TKE) and in addition investigate the influence of the slpoe angle on the production of turbulence. There has already been one thesis by Sébastian Blein and Philibert Alban focusing on the velocity profiles and the modelling of these winds on the contrary to this work, which will focus on the different surface fluxes and the turbulence kinetic energy on different levels.
We aim at completing the previous analysis and hope to improve the parametrization of large-atmospheric modelling in alpine regions, improve the accuracy of weather forecasting and provide information of the influence of katabatic winds to air quality.

2 Theory

2.1 Navier Stokes Equation

The balance of all the forces in the earth's atmosphere following a cartesian coordinate system without considering the centrifugal force are well described by the Navier Stokes Equation:

$$\frac{\partial u}{\partial t} = -u\frac{\partial u}{\partial x} - v\frac{\partial u}{\partial y} - w\frac{\partial u}{\partial z} - \frac{1}{\rho}\frac{\partial p}{\partial x} + fv + \nu\Delta u \tag{1}$$

$$\frac{\partial v}{\partial t} = -u\frac{\partial v}{\partial x} - v\frac{\partial v}{\partial y} - w\frac{\partial v}{\partial z} - \frac{1}{\rho}\frac{\partial p}{\partial y} + fx + \nu\Delta v \tag{2}$$

$$\frac{\partial w}{\partial t} = -u\frac{\partial w}{\partial x} - v\frac{\partial w}{\partial y} - w\frac{\partial w}{\partial z} + g + \nu\Delta w \tag{3}$$

where u is the horizontal wind in the x - direction (east) and v is the horizontal wind in the y - direction (north) and w is the vertical wind direction; p is the atmospheric pressure; f is the Coreolis parameter, g is the acceleration of gravity; ρ is the air density; ν is the kinematic viscosity of air and Δ is the the Laplace operator. Furthermore each term represents a certain process; from left to right they are tendency, advection, pressure gradient force, Coriolis force and the (molecular) stress. Dependent on the application one or more terms can be neglected: For example the derivation after the time $\frac{\partial}{\partial t} = 0$ if it is a steady flow or the flow is above horizontally homogeneous surfaces the advection can be neglected. Besides the order of all the terms range in between $10^{-4}\frac{m}{s^2}$ - $10^{-3}\frac{m}{s^2}$. (Foken, 2006)

2.2 Reynolds decomposition

A certain value x can be divided in a mean $\overline{x}$ and a fluctuating part x' as shown in fig.1 below. This will be especially used to express turbulence in the atmosphere. Here it is shown for a velocity, but it is possible to apply it for example on temperature, pressure, density etc. too. (Stull, 1988)

$$u = \overline{u} + u' \tag{4}$$

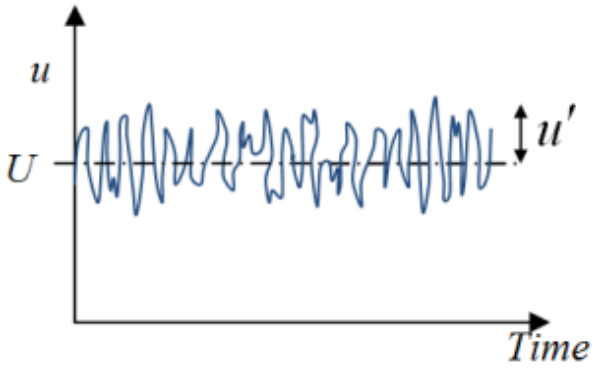

Figure 1: Reynolds decomposition (http://www.finot.com, 2018)

2.3 Covariance

To describe motions and transport of heat/velocity in the atmosphere, covariances are a very useful tool. In statistics it is defined the following way:

$$covar(A, B) = \frac{1}{N} \sum_{i=0}^{N-1} (A_i - \overline{A}) * (B_i - \overline{B}). \tag{5}$$

With the method of Reynoldsaveraging it follows that:

$$covar(A, B) = \frac{1}{N} \sum_{i=0}^{N-1} a'_i b'_i. \tag{6}$$

This means that the turbulence part of a value has the same meaning as a covariance. If you take as an example, the covariance of vertical velocity and temperature $= \overline{w'\theta'}$ on a hot summer day: We expect that the warmer than average air to rise (positive T' and w') and the cooler than average air to sink (negative T' and w'). This results in a positive covariance of $= \overline{w'\theta'}$. (Stull, 1988)

2.4 Reynolds stress

According to Stull (1988) stress is ,,the force tending to produce deformation in a body". In the atmosphere there occur three different types of stresses: pressure, Reynolds stress and viscous stress. For this project it is necessary to have a closer look on Reynolds stress.
This stress only occurs if a fluid is in turbulent motion, e.g. caused by convective processes. To demonstrate what this kind of stress is you can try to picture a cube of a certain fluid, which is exposed to different velocities on the sides. Due to these velocities the cube will be deformed. This is identical to a solid where you would apply a force on the sides of a cube and thus cause some deformation but on the contrary to a force applied on a solid we have a velocity caused by a momentum flux applied on a fluid. This momentum flux acts like a stress and is therefore called Reynolds stress. It can be as any other stress be conveyed in a stress tensor, expressed with the help of the covariance of the three velocities (Stull, 1988):

$$\tau_{x,y,z} = \begin{bmatrix} \overline{u'u'} & \overline{u'v'} & \overline{u'w'} \\ \overline{v'u'} & \overline{v'v'} & \overline{v'w'} \\ \overline{w'u'} & \overline{w'v'} & \overline{w'w'} \end{bmatrix} \tag{7}$$

The unit of this stress is $\frac{m^2}{s^2}$ and thus it is compared to e.g. pressure not a true stress. Furthermore it has to be mentioned that this tensor is a property of the flow and not of the fluid and that it is symmetric. (Stull, 1988).
However for this work we do not need the whole stress tensor. In fact, the surface Reynolds stress is needed, because its magnitude proves to be an important scaling variable. It is composed by

$$\tau_{xz} = -\overline{\rho} \overline{u'w'} \tag{8}$$

and

$$\tau_{yz} = -\overline{\rho}\overline{v'w'}. \tag{9}$$

Thus the surface Reynolds stress is computed the following way (Stull, 1988):

$$\tau_{Reynolds} = (\tau_{yz}^2 + \tau_{xz}^2)^{0.5} \tag{10}$$

2.5 Sensible Heat Flux

The sensible heat flux describes the vertical transport of temperature in the boundary layer and is governed by

$$H = \rho c_p \overline{w'\theta'}, \tag{11}$$

with ρ for the density, c_p forthe heat capacity and the covariance $\overline{w'\theta'}$.
To get a better understanding it is useful to imagine a night with cold air close to the ground and a positive temperature gradient over the height z. This means the air gets constantly warmer over the height. Now, there is due to an eddy a cold air parcel close to the ground forced to move in the positive direction upwards. This will result in cold air surrounded by warmer air and the heat flux will be negative. But the other way around works too. If there is a warm air parcel forced to move in the negative direction downward due to some eddy it will result in cold air surrounding the warm air parcel and the sensible heat flux will be again negative. (Stull, 1988)

2.6 Turbulence Kinetic Energy

Turbulences are a flow regime which is characterized by chaotic changes in pressure and flow velocity (Batchelor, 2001). The size ranges from kilometres to a few millimetres. Furthermore they can be imagined as air parcels with largely uniform thermodynamic characteristics. The largest turbulence in the atmosphere are caused by pressure differences resulting in so called eddies. These eddies feed smaller eddies and so on. Finally the eddies reach a millimetre size and disappear by the dissipation of energy due to viscosity. (Foken, 2006) A scheme of the energy cascade is illustrated in fig.2. Furthermore with increasing frequency k the turbulence are at first gaining energy in the energy conatining range. If the frequency increase even more turbulence will loose energy in the inertial subrange and with further increase it will reach the dissipation range, where the energy dissipates very fast. (Foken, 2006)

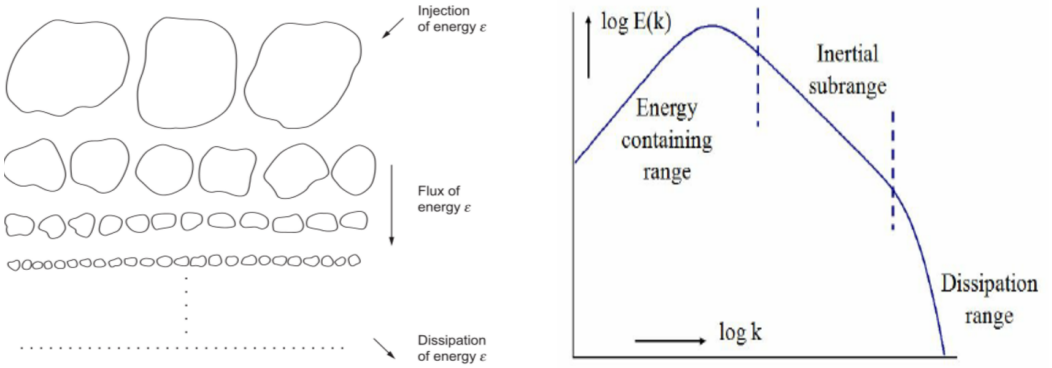

(a) https://www.quora.com, 2018 (b) https://www.researchgate.net/figure, 2018)

Figure 2: the decreasing size of turbulences (a) and the energy dissipation range (b)

In order to characterize fluctuations or turbulences of certain parameters the Reynolds decomposition is a very useful method.
To investigate the turbulent kinetic energy, firstly the kinematic energy as defined by (Stull, 1988) is needed:

$$\overline{e} = 0.5(\overline{u}'^2 + \overline{v}'^2 + \overline{w}'^2) \tag{12}$$

Furthermore the Boussinesq approximation is needed, which neglects density fluctuations but not in the buoyancy (gravitation) term:

$$\frac{\partial u_i}{\partial t} + \frac{\partial}{\partial x_j}(\overline{u_j}\,\overline{u_i} + \overline{u_j}'\overline{u_i}') = -\frac{1}{\rho}\frac{\partial \overline{p}}{\partial x_i} + \nu\frac{\partial^2 \overline{u_i}}{\partial {x_i}^2} + g\delta_{i3} + \varepsilon_{ijk} f \overline{u_k} \tag{13}$$

Finally the equation of the turbulent kinetic energy in kinematic form is obtained by multiplying equation (6) with u_i':

$$\frac{\partial \overline{e}}{\partial t} = -\overline{u_j}\frac{\partial \overline{e}}{\partial x_j} + \delta_{i3}\frac{g}{\overline{\Theta_v}}(\overline{u_i'\Theta_i'}) - \overline{u_i'u_j'}\frac{\partial \overline{u_i}}{\partial x_j} - \frac{\partial(\overline{u_j'e'})}{\partial x_j} - \frac{1}{\rho}\frac{\partial(\overline{u_j'p'})}{\partial x_i} - \varepsilon \tag{14}$$

the terms stand for the following processes:

- $\frac{\partial \overline{e}}{\partial t}$ = local TKE storage or tendency
- $\overline{u_j}\frac{\partial \overline{e}}{\partial x_j}$ = TKE advection
- $\delta_{i3}\frac{g}{\overline{\Theta_v}}(\overline{u_i'\Theta_i'})$ = buoyancy production or consumption
- $\overline{u_i'u_j'}\frac{\partial \overline{u_i}}{\partial x_j}$ = product from momentum flux (<0) and wind shear (>0), mechanical or shear production or loss term of turbulent energy
- $\frac{\partial(\overline{u_j'e'})}{\partial x_j}$ turbulent TKE transport
- $\frac{1}{\rho}\frac{\partial(\overline{u_j'p'})}{\partial x_i}$ = pressure correlation term
- ε = energy dissipation

Near the surface, the first, second, fifth and sixth term can be neglected, which results in the following equation:

$$0 = \delta_{i3}\frac{g}{\overline{\Theta_v}}(\overline{u_i'\Theta_i'}) - \overline{u_i'u_j'}\frac{\partial \overline{u_i}}{\partial x_j} - \varepsilon \tag{15}$$

2.7 The TKE Equation in a Slope-Following coordinate system

To apply the TKE equation on a slope, it is useful to express the governing equations in a Cartesian coordinate system align with the slope, which is inclined at an angle $\alpha > 0$. This is because the wind follows the slope. This results in a right-hand Cartesian coordinate system with the axes directed down the slope, across the slope and perpendicular to the slope. To take this change into account, the TKE equation has to be modified the following way:

$$\frac{\partial \overline{e}}{\partial t} = -<\overline{u'w'}>(\frac{\partial U}{\partial n}) + \beta(<\overline{w'\theta_v}'>)cos\alpha - <\overline{u'\theta_v}'>sin\alpha) + T - \epsilon, \tag{16}$$

where $e = (u'^2 + v'^2 + w'^2)/2$ is TKE, U is the mean along-slope wind speed, n is the coordinate normal to the slope, ϵ is the dissipation rate of the TKE, θ_v is the virtual potential temperature, $\beta = \frac{g}{\theta}$ is the buoyancy parameter (g is the acceleration due to gravity and θ the potential temperature, u,v and w are the down slope, cross-slope and the normal velocity components and the transport and pressure work terms are defined by $T = \frac{<w'e>+<w'p'>/\rho}{\partial n}$, where p' is the fluctuation of the pressure and ρ is the air density. (Grachev et al., 2014.)

The influence of the velocity/temperature distribution on the covariances:
To understand the effects of the slope angle on the TKE equation it is useful to have a look at the velocity and temperature parameters and see how their covariances behave below and above the wind speed maximum:
First of all we know that the temperature minimum is at the ground; thus the temperature gradient is throughout positive ($d\theta/dn > 0$). In addition we know that below the wind speed maximum the velocity gradient is positive ($du/dn > 0$) and that above the wind speed maximum the velocity gradient

is negative ($du/dn < 0$). This results in the covariances $< u'\theta' >< 0$ above the wind speed maximum and $< u'\theta' >> 0$ below the wind speed maximum.
To understand the vertical movements of the turbulent moments, it is practical to use physical arguments on turbulent eddy mixing. If you look below the wind speed maximum at an air parcel moving upward, it will transport slower and cooler air upward ($u' < 0$ and $\theta' < 0$) on the other hand if an air parcel below the wind speed maximum moves downward, it will result in an air parcel being warmer and faster than the ambient air ($u' > 0$ and $\theta' > 0$). This results in the covariances $< w'\theta' >> 0$ and $< w'u' >< 0$ below the wind speed maximum.
If you now look above the wind speed maximum at an air parcel moving upward, it will transport cooler and faster air to its new surroundings ($u' > 0$ and $\theta' < 0$) and if an air parcel moves downward, it will transport warmer and slower air to its new surroundings ($u' < 0$ and $\theta' > 0$). This will result in the covariances $< w'\theta' >< 0$ and $< w'u' >> 0$ above the wind speed maximum.
These changes of sign either have a increasing or decreasing effect on the TKE. In detail this means, that $< u', w' >$ is increasing the TKE below the wind speed maximum and decreasing it over the wind speed maximum. The covariance of $< w', \theta_v{}' >$ is throughout negative, so it is decreasing the TKE as well. On the contrary to the covariance of $< u', \theta_v{}' >$ which is decreasing the TKE below the wind speed maximum but increasing it above it. To allow a better understanding the covariances are shown with their expected sign in fig.3.

One interesting feature of the TKE equation to look at is the buoyancy term in equation 9 and its dependency on the slope angle. In gentle, almost flat terrain the buoyancy term will be only influenced by the covariance $< w'\theta' >$ and $< u'\theta' >$ will be insignificant due to the small α and within the accuracy of the experimental data. However in steep slopes starting from 20° the covariance $< w'\theta' >$ will play a more and more important role and must not be ignored. A comparison of these to covariances leads to the following feature of katabatic winds:

$$- < u'\theta' >> -cot < w'\theta_v{}' >, \tag{17}$$

which is only valid above the wind speed maximum. (Grachev et al., 2014) (Oldroyd et al., 2015)

2.8 Katabatic winds

Katabatic Winds can be found all over the world in any slope terrain. They appear in alpine and hill shaped regions, e.g. from the hostile environment of Antarctica to some hills in Europe. Because of their influence to high air pollution in urban areas they get a special meaning in Grenoble.

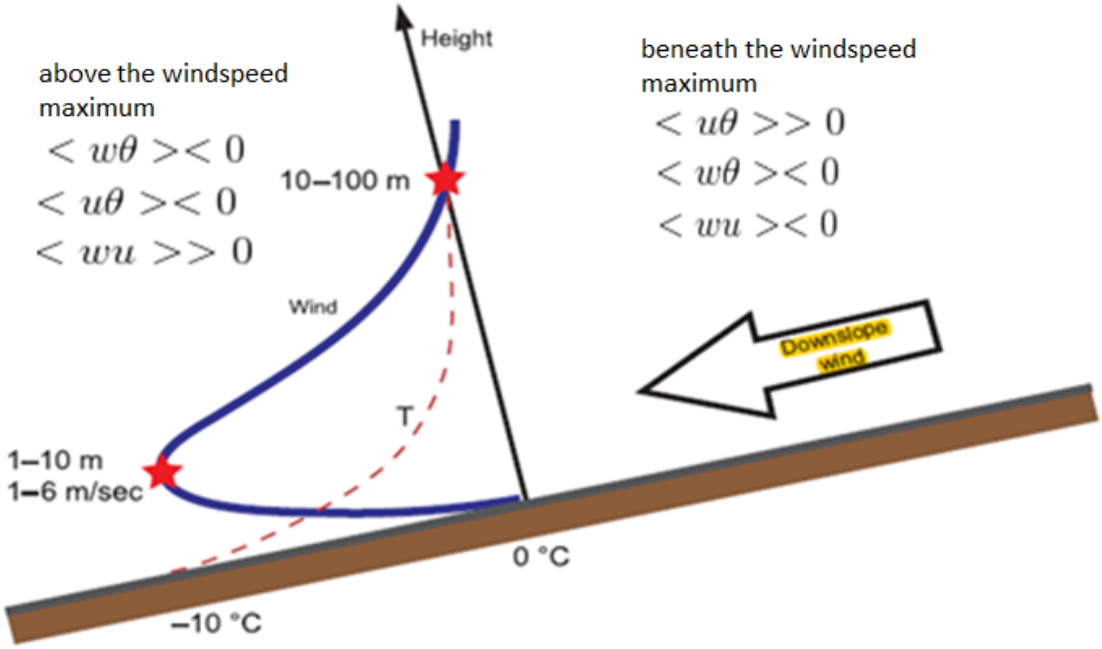

Figure 3: velocity and temperature profile of a katabatic wind (Poulos & Zhong, 2008)

Katabatic winds are generated by the following process:

The soil of a slope cools down due to a lack of radiation, for example caused by sunset. This causes a temperature difference between the soil and the air which leads to a horizontal and vertical temperature gradient. Thus the ambient air starts to cool down. This leads to an increased density of the air in contact to the soil which will be heavier than the air at the same altitude but further away from the surface. Hence there will be an unstable boundary layer with heavy cold air over light warm air, because of this the cold air starts falling down toward the valley bottom and generate a katabatic wind. Furthermore they are associated with weak large scale synoptic forcing, clear skies and form within a developing temperature inversion. However these winds appear in the lowest part of the atmosphere and have a size from a few meters to a few hundred meters with a maximum velocity very close to the surface, as can be seen in fig. 4.
In addition the temperature distribution is also shown in fig. 4 which has its minimum at the boundary to the ground and increases with the height. (Poulos & Zhong, 2008) Fig. 4 shows that the TKE rises simultaneously with the velocity, thus the turbulences depend on the velocity.
Although the process of the formation of katabatic winds is all over the world more or less the same, this work aims at a better understanding of the processes on steep slopes. The maximum wind speed is about 2 – 6 m/s at some fraction from the inversion height and decreases from this point again as can be seen in fig.4. When the cold air reaches the bottom of the valley, it will start to coagulate and will finally continue their course out valley or down valley if the valley is sloped. (Poulos & Zhong, 2008)
If katabatic winds appear on a big scale, which is for example in the Antarctica the case, the Coreolis effect has to be taken into account, which can be neglected at small scale applications. Furthermore, these winds have been researched for over 150 years now and there is a great number and variety of papers which investigate most details of them. But anyway it is still difficult to find general conclusions which apply on every type of them, because they are dependent on a large number of variables, e.g.

orientation of a valley, temperature, steepness of the slope, altitude, latitude, to only name a few. (Poulos & Zhong, 2008)

3 Methods

3.1 Measuring site

The measuring site is found at the chain of Belledone on the western side of the Grand Colon (alt.: 1770m, lat.: 45.1621, long.: 5.9138) as indicated in the fig.4 below. It is about 30km east airline away of Grenoble and is situated on a steep ($\alpha = 23°$) slope. Furthermore the snow cover is plotted in fig.5. On the first days it was still at 0.95m height, but disappeared over the observed period and it was completely gone on the 16/04.

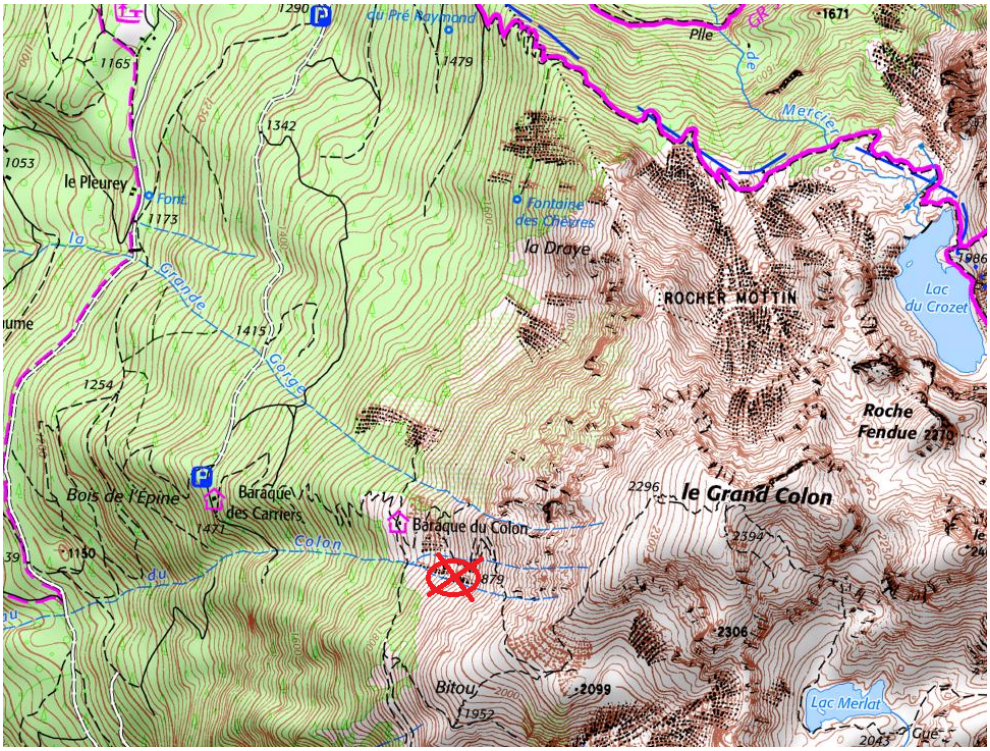

Figure 4: measuring site indicated with a red cross (geoportail.gouv.fr (2018)

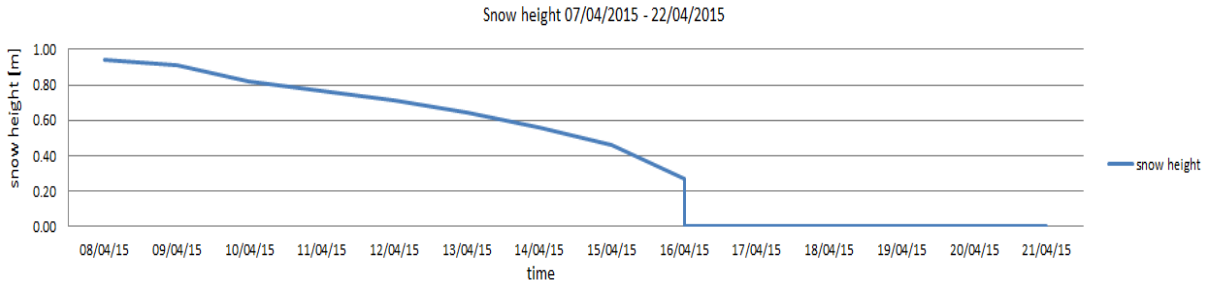

Figure 5: snow cover from 07/04 to 22/04

3.2 Equipment

The weather was observed with three sensors CS215 of the brand Campbell. These sensors were used to measure temperature and humidity with a five minute average. The reference heights are 2.16m, 5.23m and 6.78m.
Furthermore there were six sensors installed to measure velocity and temperature. Two of them were Gill Sonics of the brand Gill which generated five minutes averaged two dimensional velocity vectors. The reference heights were 1.94m and 2.39m.
The following sensors were used to receive data usable to investigate turbulences. This means the three-dimensional velocity vector was measured with a frequency of 20 Hz. The highest one, at a height of 7.29m was a Windmaster Pro also of the brand Gill. Furthermore there were three CSAT's of the brand Campbell installed. The reference heights were at 4.00m, 4.92m and 5.01m. The CSATS 2 & 3 were mounted so close o each other to receive detailed information about the gradient of the velocity.
A scheme of the measurement is shown in fig.6 and a detailed description can be found in tab.1.

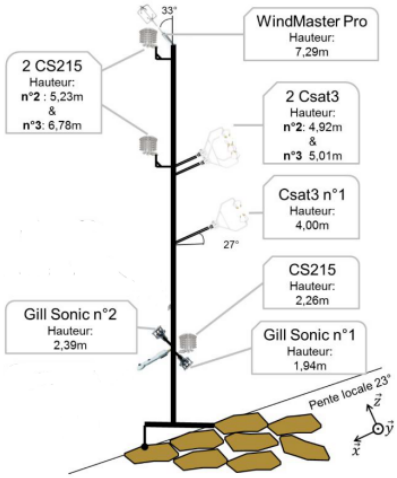

Figure 6: scheme of the measuring setup (Philibert, 2015)

sensor	parameters	frequency	initial height
CS215 No. 1	temperature, relative humidity	5min average	2.26m
CS215 No. 2	temperature, relative humidity	5min average	5.23m
CS215 No. 3	temperature, relative humidity	5min average	6.78m
CSAT No. 1	velocity (3D), temperature, pressure	20 Hz	4.00m
CSAT No. 2	velocity (3D), temperature, pressure	20 Hz	4.92m
CSAT No. 3	velocity (3D), temperature, pressure	20 Hz	5.01m
WINDMASTER	velocity (3D), temperature, pressure	20 Hz	7.29m
GILL SONIC No.1	velocity (2D), temperature	5min average	1.94m
GILL SONIC No.2	velocity (2D), temperature	5min average	2.39m

Table 1: descrition of the used probes

3.3 Data processing with Eddypro

The processing of the received turbulence data of the three CSATs and the Windmaster was done with the data processing software Eddypro. The output files of the sensors are in the ASCCI format and firstly it is necessary to allocate to each column of the raw text file a parameter (e.g. horizontal velocity, temperature). The double rotation method was chosen to rotate the wind, this means that the wind is supposed to blow parallel to the slope, which is the case of katabatic winds (and the z axis is allocated perpendicular to the ground)(Grachev et al. 2015). Furthermore, the averaging was done by the block averaging method. One time with 30 min average and one time with 5 min averaged values. To avoid spikes the spike removal option by Vicker and Mahrt (1997) was chosen and the missing values were linearly interpolated. The results are shown in several excel files and the used information including time, temperature, unrotated/rotated velocities, rotation of angle, sensible heat flux, Reynolds stress, TKE and all possible covariance in-between velocity and temperature.

3.4 Period of the Measurements

The measurements took part from 07/04/2015 until 22/04/2015.
In order to characterize pure katabatic wind it is necessary to a have a time period without any large synoptic forcing and rain. Two pluviometric stations situated in Grenoble and Chamrousse (appr. 12 and 5km away from the measuring site) show that there was rain the 16/04, the 17/04 and the 19/04. Furthermore during the measuring period there did not appear any strong synoptic wind and there could be two anticyclonic occurrences observed, from the 07/04 to the 15/04 and from the 20/04 to the 22/04. However some clouds appeared from the nights of 10/04 to 11/04. (Alban, 2015) So theoretically the nights from 07/04 to the 15/04 and the nights from the 20/04 to the 22/04 might be suitable for investigation. However a detailed look no the period will be done in the results.

4 Results

4.1 Determination of periods with katabatic winds

The developing of temperature can be seen in fig.7 (top). The graphs show the three different CS215 mounted at a height of 2.26m, 5.23m and 6.78m (green, red, blue) and the temperature of the ground (violet). After the 10/04 there develops a clear diurnal cycle with low temperatures at night (in-between -3°C and 2°C) and a fast increasing of temperature after sunrise (in-between 9°C and 14°C) and a fast decreasing of temperature after sunset. This development continues progressively until the 16/04 where the rainy period occurs, which results in only little changing temperature over day and night. Only after the 20/04 the diurnal cycle evolves again. The snow in the observed area results in a ground temperature which is during the first anticyclonic period constantly around 4°C smaller than the temperature measured by the sensor CS215 (closest to the ground). Only starting from the 17/04 the ground temperature does exceed the air temperature due to the dissapearing of the snow and only in the last two nights from the 20/04 - 22/04 the night temperature appears to be similar to a katabatic temperature profile. This results in possible pure katabatic winds from the 11/04 - 16/04 and from the nights from 20/04 - 22/04.

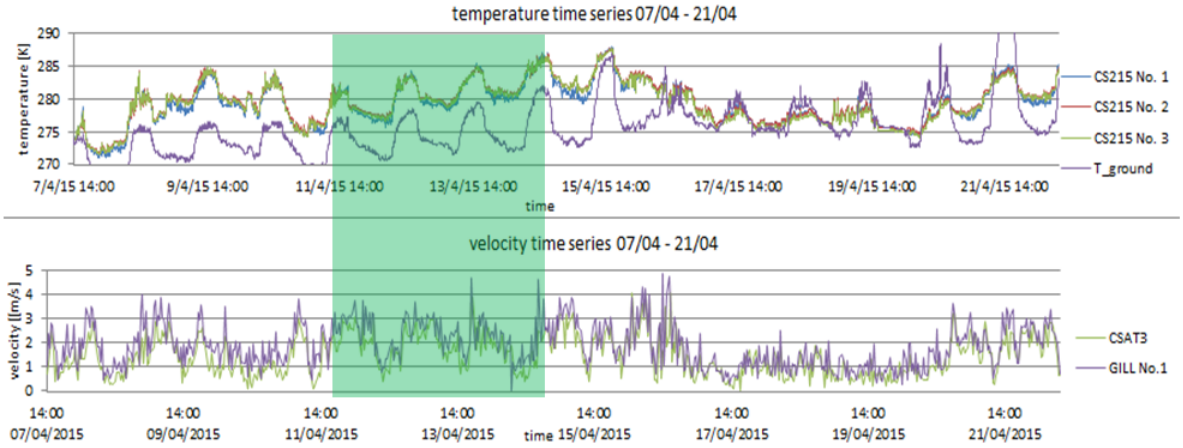

Figure 7: development of temperature over the whole measuring period (top) development of velocity over the whole measuring period (bottom)

Fig.7 (bottom) shows the development of velocity over the measured time period. Shown are the sensors GILL No.1 (violet) at a height of 1.94m and the CSAT3 (green) at a height of 5.01m. The other sensors were left out for the sake of readability. During the first period until the 16/04 the velocity is fluctuating in-between 1m/s and 5m/s. However the velocity fluctuations are usually at a minimum during daytime and reach their maximum at the nighttime. As the rainy period appears, the velocity decreases and only fluctuates between 1m/s and 2m/s. With the end of the rain the values of the velocity increase again. However it is clearly visible that the GILL sensor delivers higher velocity values compared to the CSAT3 throughout the whole measuring period, which indicates a velocity

maximum close to the ground.

All this information leaves the period from the 10/04 to the 15/04 and from the 20/04 to the 22/04. To allow a detailed look on katabatic winds and to not exceed the limits of this work I will focus on the late nights from the 11/04 to the 14/04, which are marked green in fig.7

4.2 Temperature distribution

As previously described during the three observed nights occurs a well-developed diurnal cycle with low temperatures at night and a strong increase/decrease of temperature at sunrise/sunset as can be seen in fig.8 where the time series of the CS215s and the ground temperature is plotted. Furthermore the average temperature increases progressively by 1K each day.
On fig.9 the temperature profiles are illustrated and the typical steep positive temperature gradient close to the ground is clearly visible. Above the first sensor (CS215 No.1) the temperature gradient almost disappears. In fact, over the first CSAT (at 3.20m) the temperature gradient seems to be even slightly negative. However these slight differences are exceeding the accuracy of the sensors, in addition it is difficult to compare different types of sensors at high accuracies. That is why, the temperature profiles are considered to have a positive gradient throughout the whole profile (although it is almost to zero over 3.20m). This results in a stable stratified atmosphere which leaves little room for convective processes which could disturb pure katabatic winds. Besides, Albain (2015) was facing the same issues in his work and came to the same conclusion. Furthermore you can observe that the later it got the more the curves are shifted to the left which is caused by the decreasing temperature over night.

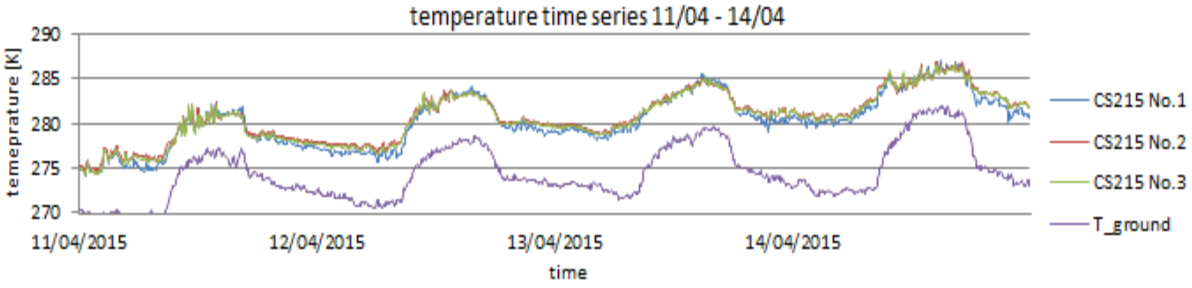

Figure 8: development of temperature from 11/04 - 14/04

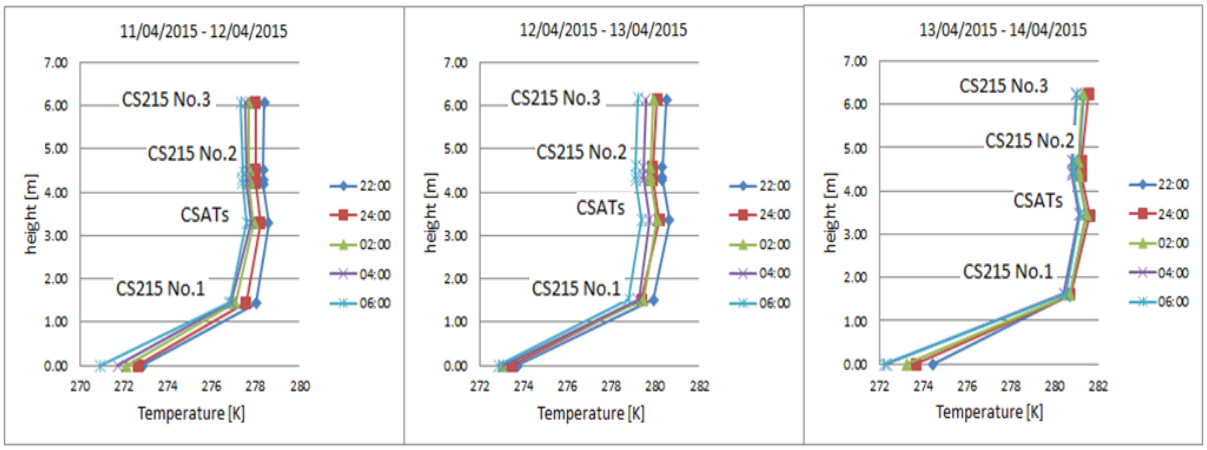

Figure 9: temperature profiles (2h average) of the three observed nights
Note for all the profiles: If the time says e.g. 22:00 it is the value from 22:00 + the averaged time period (either 30min or 2h)

4.3 Velocity distribution

Fig.10 shows the development of the velocity from the 11/04 to the 14/04. Shown are all the three CSAT's, the two GILL sensors and the Windmaster. The velocity is usually in-between $1ms^{-1}$ and $4ms^{-1}$ and are usually highest at night and reach a minimum during daytime. Furthermore the velocity of the two GILLs are almost the same and always about $0{,}5ms^{-1}$ higher than the velocity measured with the CSATs. This means the velocity maximum is close to the ground, as typical for katabatic winds.
Furthermore the wind direction as measured by CSAT1 is plotted in fig.11. During the first two nights, the rotation angle is either - 4° and -5°. However the angles of the last night are fluctuating more. They take values in-between -4° and -6°. The wind direction during the days differs up to 10° from the direction of the night.

On fig.12 the velocity profiles are illustrated. For all the three nights there is a velocity maximum close to the ground in-between 1.5 m and 2.0 m, although it is usually not very strong developed. So for the first night for example the difference between measured velocity maximum and minimum is on average around 0.5m/s. Furthermore the profile of the second night shows that the velocity gradient after the highest CSAT (at 4.55m) is slightly positive. This does not coincide with the typical features of katabatic winds. E.g. if you compare it with Grachev et al. (2014) it would be expected that above the velocity maximum close to the ground the velocity gradient would be constantly negative and descend to zero at a certain height. However a comparison with the results of Albain (2015) shows that he observed the same results. In fact he made a comparison with the model of Prandtl and found a correlation for the sensors until the first CSAT, the sensors mounted higher did not fit in this model though. It is likely that the observed katabatic wind was disturbed by ambient/largescale wind.
Besides there does no correlation between highest wind velocities and time occur. Although the velocities over the three days are all within the same range, the maximum for the first night is shared by the three curves 18:00 to 22:00 on the contrary to the last night, where the maximum occurs at 04:00 and 06:00 in the morning.

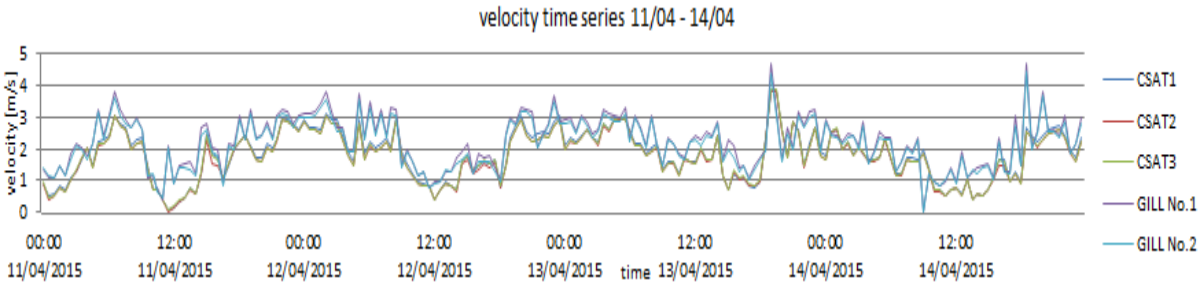

Figure 10: development of velocity from 11/04 - 14/04

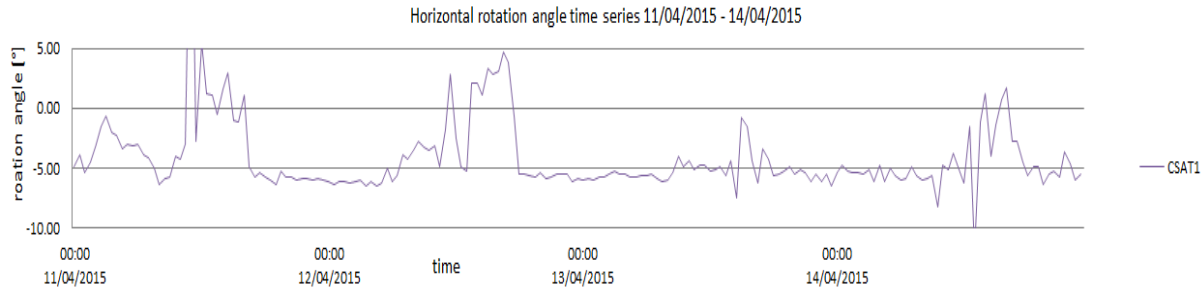

Figure 11: development of horizontal rotation angles 11/04 - 14/04

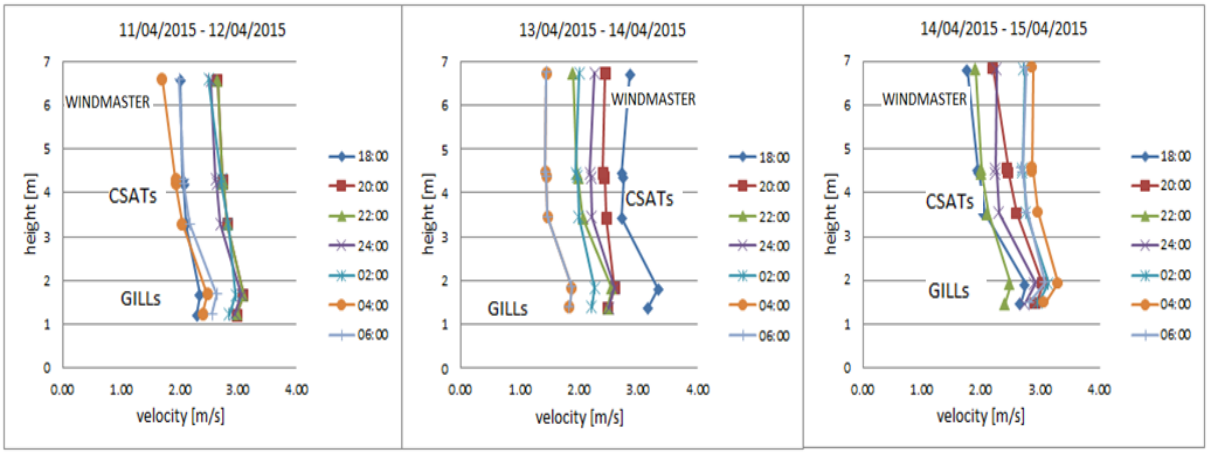

Figure 12: velocity profiles 11/04 - 14/04

4.4 Reynolds stress

The development of the Reynolds stress over the observed period is shown in fig.13. During nightime it stays at typical low values of 0.05 $kgm^{-1}s^{-2}$. With the appearance of the sun in the morning the stress at all levels rises as well. In fact it reaches values up tp 0.7 $kgm^{-1}s^{-2}$ on the first day, 0.25 $kgm^{-1}s^{-2}$ on the second and $0.65kgm^{-1}s^{-2}$ and $0.5kgm^{-1}s^{-2}$ on the last two observed days. This is caused by the radiation of the sun which heats up the atmosphere and causes instabilities in the boundary layer.
The Reynolds stress profiles are shown in fig.14. Similiar to the sensible heat flux there is a very steep gradient in-between the second and third CSAT which cannot be explained by the behaviour of the boundary layer. It is rather caused by some calibration error of the two sensors. However if we ignore this gap of Reynolds stress in-between these points, we see for the first two nights a stress which is increasing with the height and goes toward zero at the wind speed maximum. A look on the equation (12) will show us that at the velocity maximum the gradient $\partial u/\partial z = 0$ and thus the covariance $< \overline{u'w'} >= 0 >$ will be equal to zero or very little. This means that τ_{xz} is supposed to disappear and the Reynolds stress is only composed by τ_{yz}. Although we cannot say for sure, but the profiles of the first two nights show that towards the windmaximum the Reynolds stress goes almost to zero.
This does not apply for the third observed night. Here we find the Reynolds stress minimum in-between four and five meters and in addition the values of the windmaster are fluctuating in-between values of 0.04 and 0.014 $kgm^{-1}s^{-2}$. These anomalies will be discussed in the conclusion.

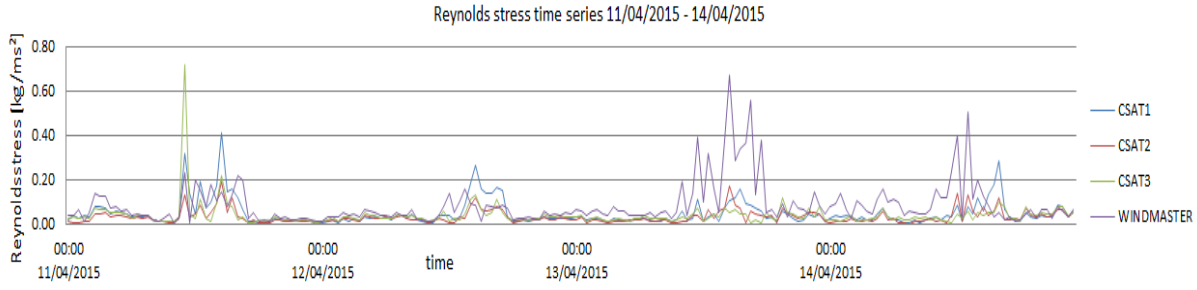

Figure 13: development of the Reynolds stress 11/04 - 14/04

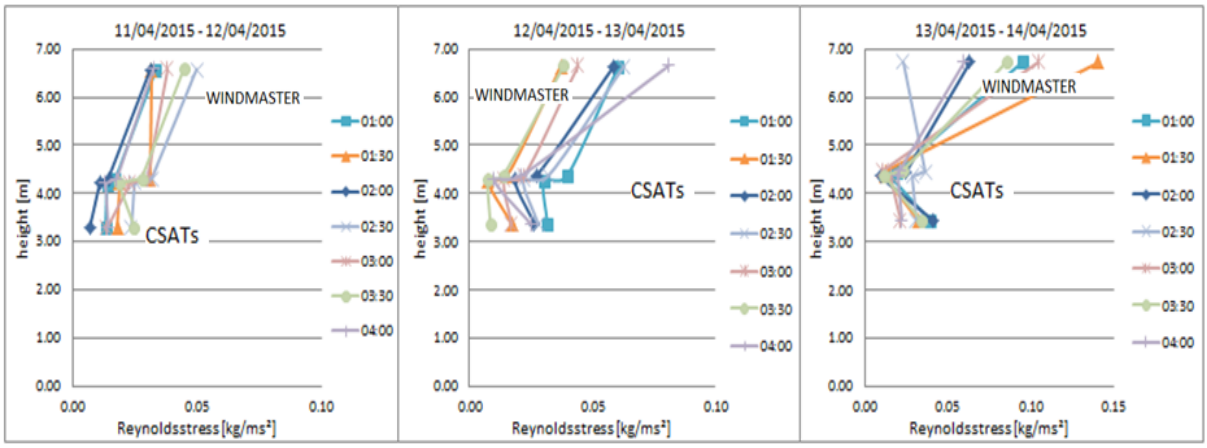

Figure 14: Reynolds stress profiles 11/04 - 14/04

4.5 Sensible heat flux

The development over time of the sensible heat flux is illustrated in fig. 15. During the first two observed nights they keep a constant value in-between -20 Wm^{-2} and -35 Wm^{-2}. After sunrise, the values are usually higher and the fluctuation increases, especially during the first day the sign changes and values over 100 Wm^{-2} are reached. This might be caused by radiative heating of the ground, which results in warm air close to the ground and a negative temperaturegradient above it. But this is still an assumption, because the ground was at that point still mostly covered with snow, which contradicts this theory. However, for the last observed night, even during the night the values are about as twice as high as the nights before.
The 30min averaged sensible heat flux profiles from 01:00 - 04:00 for each day are shown in fig.16. Conspicuous is the very steep gradient in-between the highest two CSATS, which cannot be explained by processes in the boundary layer. Same as with the Reynolds stress, this resulted rather due to some calibration errors and is not reflecting the real sensible heat flux distribution over the height. The disregard of this anomaly leads to a sensible heat flux profile which can be considered to a good approximation to be constant over the height of three meters. Same problem as with the Reynolds stress profiles, we lack unfortunately points beneath the wind speed maximum. However the constant sensible heat flux over the wind speed maximum was already observed by Grachev et al. (2015) and thus confirms the results.

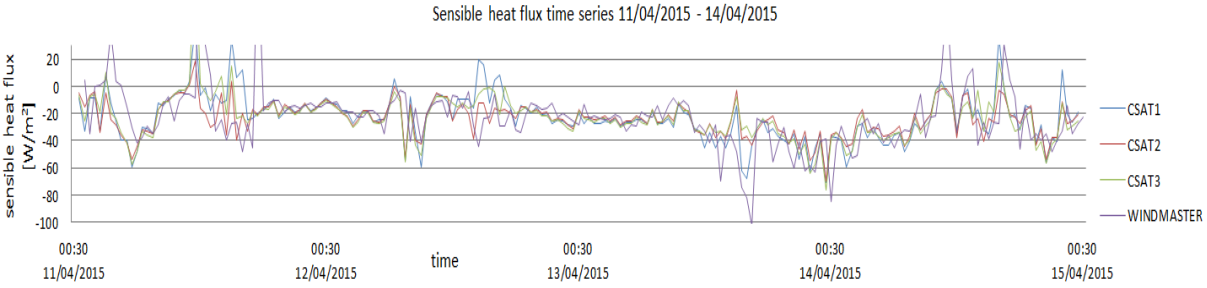

Figure 15: development of the sensible heat flux 11/04 - 14/04

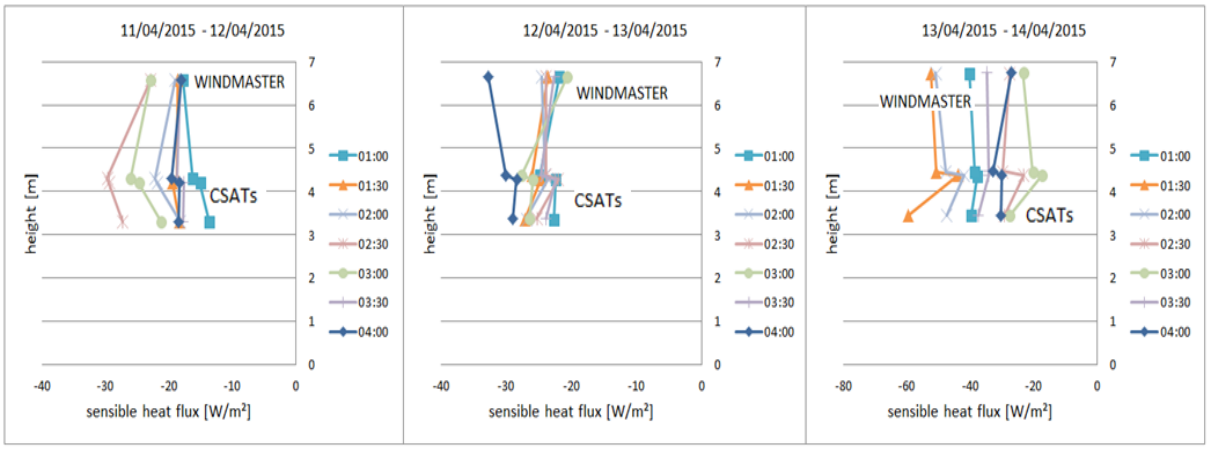

Figure 16: Sensible heat flux profiles 11/04 - 14/04

4.6 Turbulence kinetic energy

The development of TKE can be seen in fig.17. The values are in-between 1 m^2s^{-2} and 3 m^2s^{-2} during daytime and in-between 0.2 m^2s^{-2} and 1.5 m^2s^{-2} during night time. It is especially on the nights from 11/04 -12/04 and from 12/04 - 13/04 visible that TKE increases with sunrise and decreases with sunset. Furthermore all the sensors give always very similar values, except the Windmaster at a height of 6.60m (the highest sensor) which shows especially during daytime higher values which could be due to a less stable boundary layer caused by more shear in the atmosphere. Although the average velocities during daytime are lower than at night, more turbulence is observable. This is due to radiative heating of the atmosphere due to the sun. This results in more different wind directions (look fig.11) and turbulence in the atmosphere, which results in increased stress.
In fig.18 the TKE profiles from 01:00 to 04:00 with 30min averaged values for the three nights are shown. The profiles show all a very similar pattern, they have the maximum as previously mentioned at the highest measuring point at around 6.60m and the value of TKE is slowly decreasing with height.
According to equation (9) TKE will be produced by shear and the buoyancy term over the wind maximum. This results in a minimum or disappearance of the TKE at the height of the velocity maximum. Due to the fact that all the TKE data is measured above the velocity maximum, we do not have any information about what is happening beneath 3m. However the decrease of TKE over the height agrees with the predictions of Grachev et al. (2014).

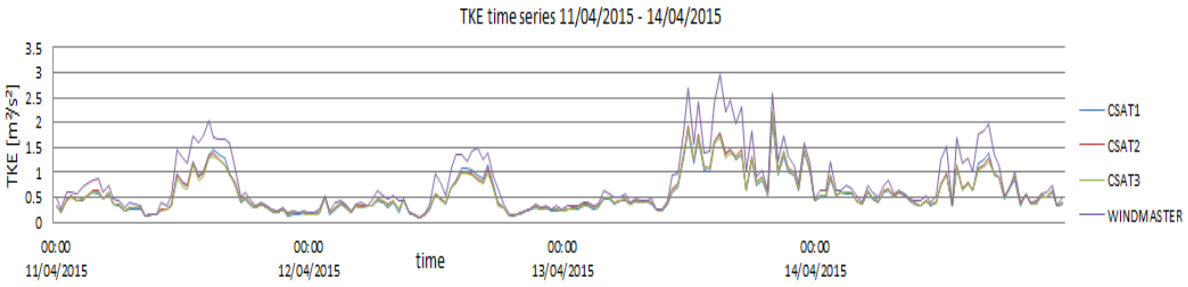

Figure 17: development of TKE 11/04 - 14/04

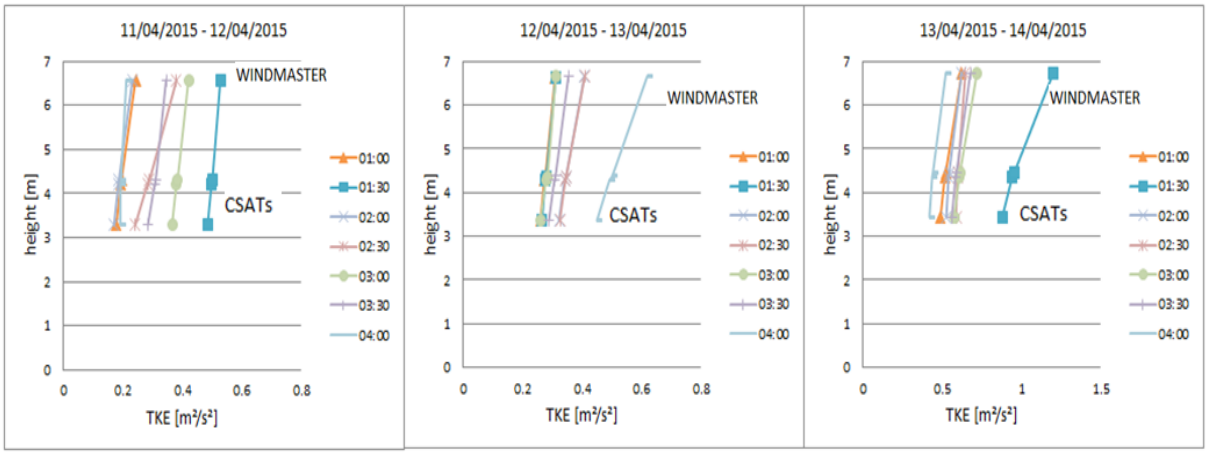

Figure 18: TKE profiles 11/04 - 14/04

Analysis of the production of TKE

As mentioned in the theory part, the production of TKE is dependent on the shear and buoyancy term, which is very dependent on the slope angle. For that reason it is necessary to have a detailed look on the covariance expressing the production shear term $- < uw > \partial U/\partial n$ and the buoyancy term of equation (9) expressed by $< w\theta > cos(\alpha)$ and $< u\theta > sin(\alpha)$. The absolute values of the production, destruction and the shear term are plotted over the first two nights in fig19.
The covariance $- < uw > \partial U/\partial n$ representing the shear term and is a production of TKE is plotted in green, the covariance $< w\theta > cos(\alpha) >$ which represents the Buoyancy destruction term of TKE is illustrated in red and $< u\theta > sin(\alpha) >$ which represents the buoyancy production term of TKE is illustrated in blue.
Over the first night the shear and the buoyancy production terms are taking very similar values around 0.03 and 0.08. On the contrary to the buoyancy destruction term which is taking very low values, not exceeding 0.05 until 06:00. This means that the TKE production is in same parts caused by the buoyancy and shear production term, which exceed at any point together the destruction of the buoyancy term. The conclusion of the second night is very similar. The production of the shear and the buoyancy term exceed the buoyancy destruction term. Although the production is mainly caused by the shear term which takes high values until 0.07. On the contrary to the buoyancy production term which is lower compared to the previous night. It takes very similar values as the buoyancy destruction term around 0.01 to 0.05 but still exceed it, except for one exception at 04:00.
In conclusion this results match together with the predictions from Grachev et. al (2014) and Oldroyd et al. (2015) that on steep mountainous slopes the TKE equation has to be modified to express the differences in the buoyancy term, because the buoyancy production term exceeds usually the buoyancy destruction term. Furthermore the production is still at least at same parts governed by the shear term.

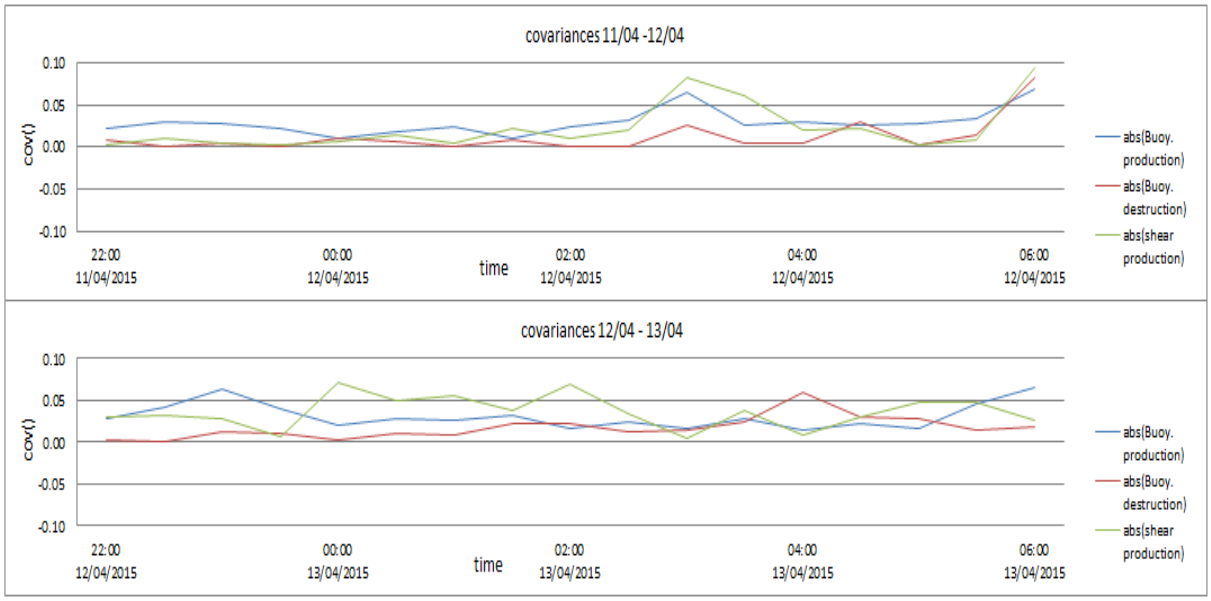

Figure 19: development of the shear, production and destruction term in the TKE equation

5 Conclusion

The results showed that the nights of the observed period from 11/04 to 14/04 were governed by katabatic winds. Although there are some occurrences in the time series and profiles which can not be explained by the occurrence of these downslope winds, namely:

- the slight negative temperature gradient in-between 3.2 and 4.2m.
- the almost vertical velocity profile over 3m
- the high Reynolds stress and sensible heat flux at the end of the 13/04
- the high spreading of Reynolds stress on the night from 13/04 to 14/04
- the compared to the nights from 11/04 to 13/04 high sensible heat flux of the night from 13/04 to 14/04
- the jumps of sensible heat flux and Reynolds stress between CSAT2 and CSAT3

However it is necessary to distinguish between the first two and the last night, because the first two nights show for every investigated feature very similar values, the only two atypical things are the slight negative temperature gradient and the almost vertical velocity profile over 3m, in fact, the first observed night shows a slight negative velocity gradient and the second night shows even a slight positive velocity gradient. The slight negative temperature gradient is very likely due to inaccuracies of the sensors, probably because of some calibration error, which resulted the temperature of the lowest CSAT to be a bit too high. Note that the gradient of the highest CSATs and the CS215 fit together. The velocity gradients of the three nights cannot be explained with some calibration or measuring errors. Rather it is likely that there were some large-scale wind motions. In fact a check with www.historique-meteo.net showed that there was an average wind velocity of approximately $2ms^{-1}$ - $3ms^{-1}$, which at least could explain the high velocities at the height of 6.5m. But the winds beneath 4-5m can still be considered to be pure katabatic. Especially the last night seem to be disturbed by some large scale motion. Further evidence for these assumptions are the peaks of Reynolds stress, sensible heat flux and TKE on the evening/night of the 13/04 to 14/04, which only can be explained by shear, vertical air movement and turbulences and are fluctuating over the whole night strongly in comparison with the first two nights.
The last noticeable anomaly was the gap between the highest two CSATs in sensible heat flux and Reynolds stress. However this cannot be related to motions in the boundary layer, rather this is due to some calibration error as well.
However despite these anomalies it was still possible to determine the following characteristics of katabatic winds align with the predictions of Grachev et al. (2014) and Oldroyd et al. (2015) namely:

- constant positive temperature gradient, which is very steep close to the ground
- a velocity maximum close to the ground
- very low Reynolds stress close to the velocity maximum and an increase over height (neglecting the calibration errors)
- an almost constant sensible heat flux over the velocity maximum (neglecting the calibration errors)
- very low TKE close to the velocity maximum and an increase over height
- an essential influence of the slope angle to the production of TKE

Unfortunately the measurements of katabatic winds were cancelled this year due to a lack of a suitable measuring period. However for future observations of these characteristics it would be a plus (if the resources allow it) to have more information about turbulences beneath the wind maximum and to investigate these downslope winds with two or even more points to receive comparable data and be even able to determine local anomalies.

6 References

Books

- Batchelor G.K.(1953). The Theory of Homogeneous Turbulence, Cambridge University Press
- Cushman Roisin B. (1994). Introduction to Gephysical Fluid Dynanics. Prentice Hall, Englewood Cliffs, New Jersey
- Foken T. (2006). Micrometeorology, Springer-Verlag Berlin Heidelberg
- Stull R. B. (1988). An Introduction to Boundary Layer Meteorology. Atmospheric and Oceanographic Sciences Library

Papers and reports

- Philibert A. (2016). Etude Expérimentale de caractérisation d'un écoulement catabatique sur forte pente. LEGI
- Blein S. (2016). Observation et modélisation de couche limite atmosphérique stable en relief complexe: le processus turbulent d'écoulement catabatique, LEGI
- Grachev A., Leo L., Di Sabatino S., Fernando H., Pardyjak E., Fairall C. (2014). Structure of Tubulence in Katabatic Flows Below and Above the Wind-Speed Maximum
- Mahrt L. (2014). Stably Stratified Atmospheric Boundary Layers. Northwest Research Associates, Oregon State University
- Oldroyd H., Pardyjak E., Higgins C., Parlange M. (2015). Buoyant Turbulent Kinetic EnergyProduction in Steep-Slope Katabatic Flow
- Poulos G. and Zhong S.(2008). An observational History of Small-Scale Katabatic winds in Mid – Latitudes. Geography Compass

Websites

- www.quora.com
- www.researchgate.net/figure
- www.finot.com
- www.historique-meteo.net

List of Figures

List of Tables